PERGAMON

International Journal of Multiphase Flow 28 (2002) 1873–1894

International Journal of Multiphase Flow

www.elsevier.com/locate/ijmulflow

# Effect of coarse particles on the heat transfer in a particle-laden turbulent boundary layer

G. Hetsroni *, A. Mosyak, E. Pogrebnyak

*Department of Mechanical Engineering, Technion-Israel Institute of Technology, 32000 Haifa, Israel*

Received 20 January 2002; received in revised form 25 September 2002

**Abstract**

The temperature distribution in particle-laden turbulent flow, in a flume, was investigated both by DNS and experimentally. Simulations were performed at $Re = 171$ and $Pr = 5.4$ in order to study the interaction between the particle motion and flow turbulence. Two-way coupling was used to obtain various turbulence statistics, the grid resolution was sufficiently fine to resolve all essential turbulent scales. The effect of particle diameter on momentum, heat transfer and particle deposition was considered. The details of particle-turbulence interaction depend on the particle Stokes number and the particle Reynolds number.

The spatial structures of instantaneous flow and temperature fields were visualized. Low frequency small oscillations of deposited particles were observed. It was found that these small deviations from the initial position, caused strong changes in the instantaneous temperature field near the particle.

The experiments provided details of the temperature field on the heated wall close to the particle. In the front of the particle, a sharp increase in heat transfer coefficient was observed. The experimental results agree well with the computational predictions.


*Keywords:* Direct numerical simulation (DNS); Turbulent flume; Coarse particles; Near-wall turbulence; Deposition; Heat transfer

## 1. Introduction

One of the most interesting problems in turbulent flows is the prediction of momentum and scalar transport in a turbulent boundary layer. In modeling turbulent flows in a boundary layer the contribution of turbulent eddy viscosity to the total (eddy plus molecular) viscosity is known

* Corresponding author. Tel.: +972-4-829-2058; fax: +972-4-823-8101.
*E-mail address:* hetsroni@tx.technion.ac.il (G. Hetsroni).

0301-9322/02/$ - see front matter 
PII: S0301-9322(02)00122-2

to be negligible at distances from the wall that are less than about 4–5 wall units. Heat transfer at *Pr* of about 5–7 shows similar behavior, where the contribution of the turbulent eddy thermal diffusivity also becomes small within such a distance from the wall (Tiselj et al., 2001). In particle-laden flows, however, the contribution of turbulence to the total diffusivity does not become negligible until a distance of about $y^+ = 0.5$ is reached (Li et al., 1999). Moreover in particle-laden flow the concentration changes are well within near-wall region for boundary layer flows (Pedinotti et al., 1992). This kind of flow occurs in many technical processes in chemical engineering, mineral processing, and energy conversion. In such processes, the fluid flow is turbulent, and the influence of particles on fluid turbulence plays a very important role in transport of momentum, mass end energy between solid and fluid phases.

Modification of turbulence characteristics by solid particles has been investigated by various numerical and experimental studies. The structure of particle distribution and turbulence in the near-wall region of a flume was examined by Pedinotti et al. (1992) using one-way coupled DNS, Pan and Banerjee (1996, 1997) and Li et al. (1999) using two-way coupled DNS. It was shown that ejection-sweep cycle is affected by particles. Application of DNS to the study of particle deposition in turbulent boundary layers by McLaughlin (1989) (Fessler et al., 1994; Eaton and Fessler, 1994; Wang and Squires, 1996) has clearly shown that heavy particles accumulate in the low velocity streaks. Yamamoto et al. (2001) reported large eddy simulation (LES) results for a channel air flow. They considered 50 μm glass particles, 70 μm copper particles and 28 μm lycopodium particles in the simulations. It was found that particles with the least inertia showed the greatest tendency to form clusters. Li et al. (2001) performed numerical simulation of particle-laden turbulent channel flow. Results are reported for glass and copper particles. The densities of glass and copper were taken to be 2.5 and 8.8 g/cm$^3$. Density of the fluid (ambient air) was $1.2 \times 10^{-3}$ g/cm$^3$. The values of $\rho_p/\rho_f$ for glass and copper particles were 2083 and 7333, respectively.

The equations used in calculations of particle deposition in turbulent boundary layers describe the motion of particles with densities substantially higher than that of the surrounding fluid, and diameters small compared to the Kolmogorov scale. Armenio and Fiorotto (2001) showed that pressure drag is relevant only for $(\rho_p/\rho_f) \sim 1$ and it drops with increasing density ratio. However, it should be pointed out that the deposition of particles with density ratio $(\rho_p/\rho_f) \sim 1$ was not studied.

A review of experimental studies of turbulence modification by particles is given by Gore and Crowe (1991). The authors showed that the ratio of particle diameter and turbulence length scale is an appropriate measure to decide if the turbulence intensity of carrier fluid is augmented or attenuated by dispersed particles. However, the data are scattered and indications about the degree of increase or decrease versus flow condition are not provided. The structure of particle distribution and turbulence in the near-wall region was observed by Rashidi et al. (1990), Kaftori et al. (1998) using oxygen bubble visualization for the particle-laden flow of water in a flume. They found that particles are affected by coherent wall structures and tend to form streaky structure in regions of low fluid velocity. The interactions between small dense particles and fluid turbulence have been investigated by Kulick et al. (1994) in a down flow fully developed channel in air. Particles velocities and fluid velocities in the presence of 50 μm glass, 90 μm glass and 70 μm copper spherical beads were measured at particle mass loading up to 80%. These particles were smaller than the Kolmogorov length scale.

Hetsroni and Rosenblit (1994) and Hetsroni et al. (1995, 1997) used infrared thermography to study the thermal interaction between the particle-laden turbulent flow and a heated plate, and

heat transfer enhancement by a sphere attached to the bottom of the flume. Recently Hetsroni et al. (2001a) studied the effect of particle motion on turbulence and heat transfer and compared the results to those produced by a stationary particle. It was shown that enhancement of heat transfer coefficient depends on the ratio of the particle Reynolds number (based on the particle diameter and relative flow velocity), to the shear Reynolds number (based on the particle diameter and shear velocity). But the differences of the flow fields and thermal pattern with and without the effect of particle deposition were not examined.

### 1.1. Objectives and outline

The present study differs in several respects from those of Kulick et al. (1994) (Wang and Squires, 1996; Yamamoto et al., 2001; Li et al., 2001). The coarse particles were used in the DNS and experiments, so that the effect of nonuniform velocity field on particle-turbulence interaction near the wall was accurately represented. The particles have low density ratio and the effects of drag and lift forces are important. Much of the present paper focuses on the effects of particles on heat transport in the turbulent boundary layer. We calculated water flow in a flume by DNS with two-way coupling in order to consider the effect of the particle diameter at density ratio $(\rho_p/\rho_f) \sim 1$ on momentum and heat transfer in the near-wall region. In particular, the effect of the behavior of a single particle under condition of particle deposition was analyzed and compared with experimental results. In the present study the analysis of the statistics of coherent structures is focused mainly on a region near the wall. In this region corresponding to $y^+ < 40$, coherent structures account for over 80% of the energy in the turbulent fluctuations (Lumley and Blossey, 1999).

## 2. Mathematical description

### 2.1. Flow field

We examine, by two-way coupling, the interaction between large particles ($Re_p > 1$) and the turbulence in the near-wall region of a flume, here $Re_p = dU_c/v$, $U_c$ is the mean velocity of the fluid on the streamline through the center of sphere. The time-dependent, three-dimensional Navier–Stokes and continuity equations are solved in a rectangular domain. The flow geometry and coordinate system is sketched in Fig. 1. The basic equations solved for the flume are

$$\nabla \bar{u} = 0 \tag{1}$$

$$\frac{\partial \bar{u}}{\partial t} = -\nabla(\overline{uu}) + v\nabla^2 \bar{u} - \frac{1}{\rho}\nabla p \tag{2}$$

where $t$ is time, $v$ is kinematic viscosity, $\rho$ is density, $p$ is pressure, with boundary conditions $u = w = v$ (no-slip) at the bottom wall and, $\partial u/\partial y = \partial w/\partial y = 0$, $v = 0$ at the free surface. Eqs. (1) and (2) and boundary conditions have been made dimensionless using the friction velocity $u^*$, $(u^* = (\tau/\rho)^{0.5})$ where $\tau$ is wall shear stress. Periodic boundary conditions are used in streamwise

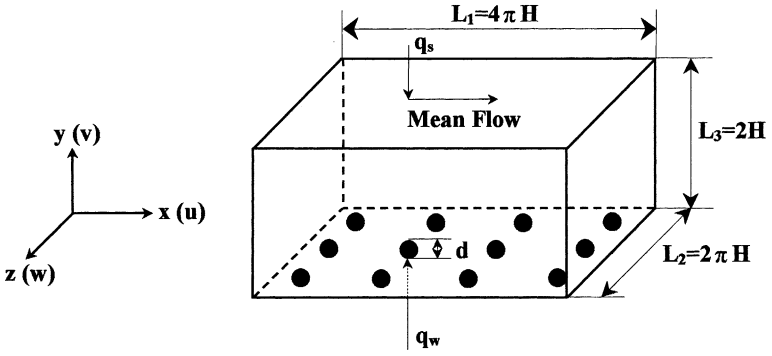


Fig. 1. Computational domain and coordinate system.

($x$) and spanwise ($z$) directions. The initial conditions are the mean profiles for the velocity, superimposed with sinusoidal perturbations.

A pseudo-spectral method is employed to solve the governing equations. In the homogeneous ($x$ and $z$) directions, all the quantities are expressed by Fourier expansions. In the wall-normal direction $y$, which is nonhomogeneous, they are represented by Chebyshev polynomials. Numerical procedure and the code of Gavrilakis et al. (1986), modified by Lam and Banerjee (1988) were upgraded (Li et al., 1999; Tiselj et al., 2001) and used to solve the continuity and momentum equation.

In the present study, the turbulent channel flow of Reynolds number ($Re = u^*2H/\nu$), $Re = 171$ and $Pr = 5.4$ is simulated. The bulk Reynolds number $Re_B = 2Hu_B/\nu$ in this case is about 2600, where $2H$ is the flow depth, $2H = 37$ mm, and $u_B$ is the bulk streamwise velocity, $Pr$ is the Prandtl number. The calculations were carried out in a computational domain of $1074 \times 171 \times 537$ wall units in the $x$, $y$ and $z$ directions with a resolution of $128 \times 65 \times 128$. A nonuniform distribution of collocation points is used in the wall-normal ($y$) direction due to the nature of the Chebyshev polynomials, and the first collocation point is at $y^+ = 0.1$ away from the wall.

The DNS in the computational volume of $1074 \times 171 \times 537$ wall units (in the $x$, $y$, and $z$ directions, respectively) gave sufficiently accurate statistics and two-point correlation. This choice of the dimension of the computational domain is large enough to include the expected scales of the largest structures in the flow, and is in line with recent numerical studies as discussed below. The streamwise and spanwise size used in the present study is large enough to allow about five streaks in the spanwise direction and about 1–2 in the streamwise direction. Note that the numerical experiments by Pedinotti et al. (1992), Pan and Banerjee (1996, 1997) suggest that the domain sizes used in the present work are sufficient, also for particle-laden flow if the averaged volume fraction of the solid particles is less than $10^{-3}$. Their calculations were carried out in a computational domain of $1073 \times 171 \times 556$, wall units in the streamwise, wall-normal and spanwise directions, respectively. The bulk Reynolds numbers based on the mean streamwise velocity and the depth of the channel were 2500 and 5000. The authors varied particle size over a wide range from 1 to 17 wall units, and did not observe "locking" of particles into streaks, due to the periodic boundary conditions being applied in the streamwise direction.

After the flow field is brought to a stationary state, the spherical particles of density 1050 g/cm$^3$ and of diameter $d^+ = 8.5$ or $d^+ = 17$ are introduced into the flow, where $d^+ = du^*/\nu$, $d$ is the

sphere diameter. The number of particles was 160 and 16, so that the volume concentration was $C_1 = 5.2 \times 10^{-4}$ and $C_2 = 5.2 \times 10^{-4}$ for particles of $d^+ = 8.5$ and $d^+ = 17$, respectively.

The approximate form of the equation for the motion of a spherical particle is

$$m_{\mathrm{sp}} \frac{\mathrm{d}\bar{v}}{\mathrm{d}t} = \frac{3}{4} C_{\mathrm{D}} \frac{\rho}{\rho_{\mathrm{sp}}} \frac{1}{d_{\mathrm{sp}}} |\bar{u} - \bar{v}| m_{\mathrm{sp}} (\bar{u} - \bar{v}) f(G) + m_{\mathrm{f}} \frac{\mathrm{D}\bar{u}}{\mathrm{D}t} + \frac{1}{2} m_{\mathrm{f}} \frac{\mathrm{d}}{\mathrm{d}t} (\bar{u} - \bar{v}) + (m_{\mathrm{sp}} - m_{\mathrm{f}}) \bar{g} + 6\pi \left( \frac{d_{\mathrm{sp}}}{2} \right)^2 \mu \int_{t_0}^{t} \frac{\mathrm{d}}{\mathrm{d}\tau} (\bar{u} - \bar{v}) [\pi \nu (t - \tau)]^{-0.5} \, \mathrm{d}\tau \tag{3}$$

where drag coefficient is given by

$$C_{\mathrm{D}} = \frac{24}{Re_{\mathrm{sp}}} + \frac{6}{1 + Re_{\mathrm{sp}}^{0.5}} + 0.4, \quad 0 < Re_{\mathrm{sp}} < 2 \times 10^5 \tag{4}$$

Pan and Banerjee (1997) compared the drag coefficient, $C_{\mathrm{D}}$, from their simulation with that of an empirical formula (4) obtained by White (1991). Eq. (4) agrees with DNS carried out by Pan and Banerjee (1997) with a standard deviation of 1%.

$Re_{\mathrm{sp}}$ is the Reynolds number of sphere

$$Re_{\mathrm{sp}} = \frac{|\bar{u} - \bar{v}| d_{\mathrm{sp}}}{\nu}$$

$m_{\mathrm{sp}}$ is the mass of the sphere, $\mu$ is the fluid viscosity, $\bar{v}$ is the velocity of the sphere, $f(G)$ is the coefficient of wall effect on the Stokes drag, $G$ is the distance from the center of the sphere to the wall, $m_{\mathrm{f}}$ is the mass of the fluid displaced by the sphere, $\bar{g}$ is the acceleration due to gravity, $\mathrm{d}/\mathrm{d}t$ is the time rate of change following the sphere, $\mathrm{D}\bar{u}/\mathrm{D}t$ is the total acceleration of the fluid by the sphere. $\mathrm{D}\bar{u}/\mathrm{D}t = \partial\bar{u}/\partial t + \bar{u}\nabla\bar{u}$, instantaneously evaluated at the particle position. The coefficient of wall effect is given by Kim and Karrila (1991) for a particle moving parallel to a wall

$$f(G) = \frac{1}{1 - \frac{9}{16} \frac{d_{\mathrm{sp}}}{2G} + \frac{1}{8} \left( \frac{d_{\mathrm{sp}}}{2G} \right)^2} \tag{5}$$

and for a sphere moving perpendicular to a wall

$$f(G) = \frac{1}{1 - \frac{9}{8} \frac{d_{\mathrm{sp}}}{2G} + \frac{1}{2} \left( \frac{d_{\mathrm{sp}}}{2G} \right)^2} \tag{6}$$

Issues with regard to dilute suspensions of particle can be divided into how particles distribute in a turbulent field and how particles affect the turbulent flow field, i.e. the "two-way coupling" problem. We consider the flow of incompressible fluids governed by the Navier–Stokes equations with an external force field as

$$\frac{\partial \bar{u}}{\partial t} = -\nabla(\overline{uu}) + \nu \nabla^2 \bar{u} - \frac{1}{\rho} \nabla p + S_{\mathrm{pi}} \tag{7}$$

where $S_{\mathrm{pi}}$ represents the external force for modeling the no-slip boundary condition on the solid sphere in the flow. In this context $S_{\mathrm{pi}}$ is the force exerted by the body on the fluid. For a given flow with no-slip boundary conditions, there exists a force on the surface, which if applied at the

boundary, which brings the flow to rest at each point of the bounding surface. Where a stationary solid body is introduced into a steady fluid flow, the values of the fluid velocity on the boundary of the body are equal to zero. If the spheres were moving, the values of fluid velocity and body velocity must be equal.

A successful method for modeling of the no-slip boundaries with an external force field for the pseudo-spectral numerical scheme was described by Goldstein et al. (1993). The results of the numerical simulation of the interaction between solid particles and near-wall turbulence were presented by Li et al. (1999). It was shown that the large particles significantly affect mean velocity profile and statistics of velocity fluctuations.

### 2.2. Temperature field

The energy equation is

$$\frac{\partial T}{\partial t} = -\nabla(uT) + \alpha\nabla^2 T \tag{8}$$

where $T$ is the temperature, $\alpha$ is the thermal diffusivity. The temperature in Eq. (8) is treated as a passive scalar.

The boundary conditions are the heat flux $q_w$ is equal to constant on the bottom wall, and heat flux $q_s = 0$ at the free surface. The expression "isoflux boundary condition ($q_w = \text{constant}$)" means that the wall temperature fluctuations are not zero. It was shown by Tiselj et al. (2001) that under isoflux condition the temperature field exhibits more anomalies compared to the isothermal wall boundary condition. The problem of the isoflux wall boundary condition is the ill-posedness of the energy equation. In the present work ill-posedness is removed by additional constraint, which is imposed on the heated wall. The time and space averaged dimensionless wall temperature difference is zero.

The heating condition of the constant mean heat flux along the bottom of the flume is equivalent to an assumption that the wall temperature ensemble-averaged over the $z$ direction and time should increase linearly in the $x$ direction (Kasagi et al., 1992). As a result, the bulk mean temperature should also increase linearly in the $x$ direction. The mean temperature gradient in $x$ direction can be expressed with wall heat flux, if the global energy balance is written for the averaged conditions in the channel volume $2HL_1L_2$, heated bottom surface $L_1L_2$ and in the time which the fluid travels with the bulk velocity $u_B$ crosses the distance $L_1$

$$(2HL_1L_2)\rho c_p \Delta T = q_w(L_1L_2)(L_1/u_B) \tag{9}$$

So the mean temperature gradient is

$$\frac{\Delta T}{L_1} = \frac{q_w}{2H\rho c_p u_B} \tag{10}$$

The bulk velocity is defined as

$$u_B = \frac{1}{2H}\int_0^{2H} \langle u_1 \rangle_{x,z,t} \, dy \tag{11}$$

where $\langle u_1 \rangle_{x,z,t}$ means averaging over $x, z$ and time $t$.

The code was also upgraded with the dimensionless energy equation

$$\frac{\partial\theta^+}{\partial t^+} = -\nabla(\bar{u}^+\theta^+) + \frac{1}{RePr}\nabla^2\theta^+ + \frac{u^+}{2u_B^+} \tag{12}$$

derived by Kasagi et al. (1992), Kawamura et al. (1998) with dimensionless wall temperature difference

$$\theta^+(x,y,z,t) = (\langle T_{WALL}\rangle - T(x,y,z,t))/T^* \tag{13}$$

In Eqs. (9) and (10) $\bar{u}^+ = (u^+, v^+, w^+)$ represents the velocity vector normalized with the friction velocity $u^*$, $T^* = q_w/\rho c_p u^*$ is friction temperature, $q_w$ is time averaged wall heat flux, $c_p$ is specific heat at constant pressure. time and space averaged dimensionless wall temperature difference is fixed to zero $\langle\theta^+_{WALL}\rangle = 0$.

We assume there is no heat transfer between the sphere and the fluid. In the applied pseudo-spectral scheme the wall boundary condition is implemented in the last step of the algorithm, where the temperature is found as a solution of the differential equation of the Helmholtz type

$$\left(\frac{d^2}{dy^2} - \frac{1+\alpha k^2}{a}\right)\theta^+ = \mathrm{He}(y) \tag{14}$$

This equation with $\alpha = \Delta t^+/(2RePr)$, $k = \sqrt{k_x^2 + k_z^2}$, and $\mathrm{He}(y)$ containing nonlinear terms and contribution of the old time step, is solved in the wall-normal (Chebyshev) direction for each pair of wave numbers $(k_x, k_z)$. The boundary condition at the free surface is $d\theta^+/dy = 0$. The isothermal boundary condition at the wall is $\theta^+ = 0$. For isoflux boundary condition at the wall Eq. (11) is solved with the boundary conditions

$$\begin{aligned} &\theta^+ = 0 \quad \text{for } k_x = k_z = 0 \\ &\frac{d\theta^+}{dy^+} = 0 \quad \text{for all other pairs of } k_x, k_z \end{aligned} \tag{15}$$

Such boundary condition fixes the average wall temperature (which corresponds to the zero wave number) to zero, and at the same time allows free fluctuations of the other temperature components.

The temperature fluctuations may be determined by the coupled unsteady heat conduction inside the wall, so that they cannot be specified without knowing the wall material and its thickness. This conjugate heat transfer problem was studied by Kasagi et al. (1989). The particular case of wall thickness $\delta = 0$ corresponds to ideally isoflux wall with infinitesimally small wall thickness. The case of an ideal isoflux wall is used in the present study to estimate those wall temperature fluctuations that could be realistically expected for a very thin wall.

Any buoyancy effect was neglected, and hence the temperature was considered as a passive scalar. As the initial condition, a uniform temperature field was projected on the velocity field. The heat transfer simulation was started after the velocity field had reached a steady state. Then once the velocity field was calculated at each time step, the temperature field was obtained by integrating the energy equation with the same grid system used for the velocity field.

The computation proceeded until the temperature field was estimated to be fully developed. Next, the procedure was started in order to obtain statistical data about the temperature. Finally,

the instantaneous temperature fields were used as an initial database for the main computation after all statistical quantities were obtained. The grid resolution, the time increment and all the schemes of the preliminary computation were the same as those in the main computation. The time integration was repeated for about 2500 $v/u^{*2}$ and then the computation was further continued for about 700 $v/u^{*2}$ (20,000 time steps) in order to calculate turbulence statistics as ensemble averages over space and time. The data sampling was started when we observed stationary time histories of the statistics. The numerical accuracy of DNS was validated in the previous calculations (Li et al., 1999; Hetsroni et al., 2001b; Tiselj et al., 2001).

## 3. Results of DNS simulation

### 3.1. Velocity and temperature fields

#### 3.1.1. Near-wall thermal pattern

The Stokes number and particle diameter significantly affect the particle behavior in the near-wall region. It is reasonable to believe that details of instantaneous scalar field structure advected by fully developed turbulent flow would reflect these features. Fig. 2a shows the instantaneous temperature field in the $x^+$–$z^+$ plane ($y^+ = 4.9$) for flow with particles $d^+ = 8.5$. Fig. 2b shows the instantaneous temperature field in the $x^+$–$z^+$ plane ($y^+ = 8.2$) for flow with particles $d^+ = 17$ the heat flux was $q = 10^4$ W/m$^2$. It shows that the particles are stopped. A closer examination shows small deviations from the initial positions.

Depending on particle diameter we find that the behavior of particles close to the bottom of the flume is quite different. For $d^+ = 17$ the particle deposition takes place and these particles almost do not move in the flow direction. One of the cause of this difference is the relation of the particle relaxation time, $\tau_p$, to the characteristic time scale of fluid turbulence, $\tau_f = v/u^{*2}$. The Stokes number, $St^+ = \tau_p u^{*2}/v$, is a parameter often used to represent the influence of particles on fluid turbulence (Yamamoto et al., 2001). When the value of $St^+$ is 0, particles completely follow the fluid motion as ideal traces, while at very large Stokes number particles do not move by carrier fluid. Under condition of the present DNS the Stokes number depends only on particle diameter: for $d^+ = 8.5$ the value of Stokes number is $St^+ = 4.22$, for $d^+ = 17$ Stokes number is $St^+ = 16.9$.

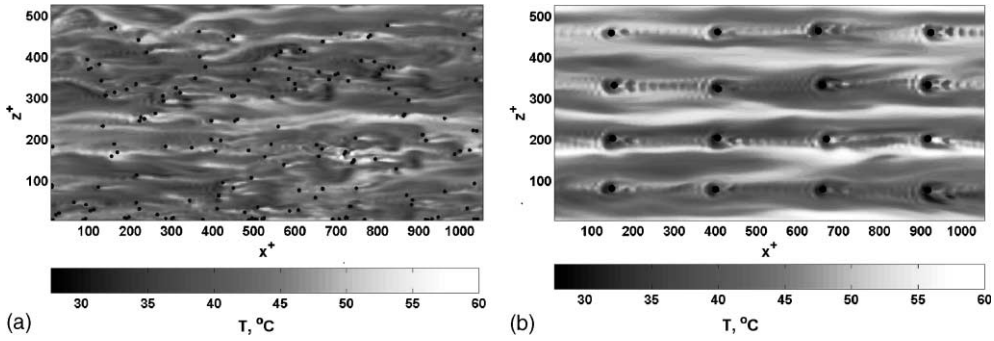


Fig. 2. Instantaneous temperature field in the $x^+$–$z^+$ plane: (a) $d^+ = 8.5$, $y^+ = 4.2$, (b) $d^+ = 17$, $y^+ = 8.5$.

The present results agree with observations by Nino and Garcia (1996). They showed that particles of sizes larger than the thickness of about $y^+ = 10$ were not picked up by flow ejection events.

Analysis of motion pictures showed low frequency small oscillations of deposited particles. The displacement of particles did not exceed 2 wall units, the dimensionless frequency of oscillations was about $f^+ = 0.01$. Fig. 3a shows instantaneous temperature distribution on the heated wall-near the sphere of $d^+ = 17$. Fig. 3b shows it after time interval $\Delta t^+ = 500$. The flow is from the right to the left, the temperature scale is from 30 to 60 °C. The changes in thermal pattern are due to displacement of the sphere. Comparison with the experiment, presented below, showed that these changes did not have strong effect on time averaged heat transfer coefficient.

*3.1.2. Velocity distribution around the sphere of $d^+ = 17$ deposited on the bottom of the flume*

Fig. 4a indicates the vector velocities in the $x^+$–$y^+$ plane (the center of the sphere is located at the streamwise axis of symmetry). For a free stream relative to a front of the sphere two areas may

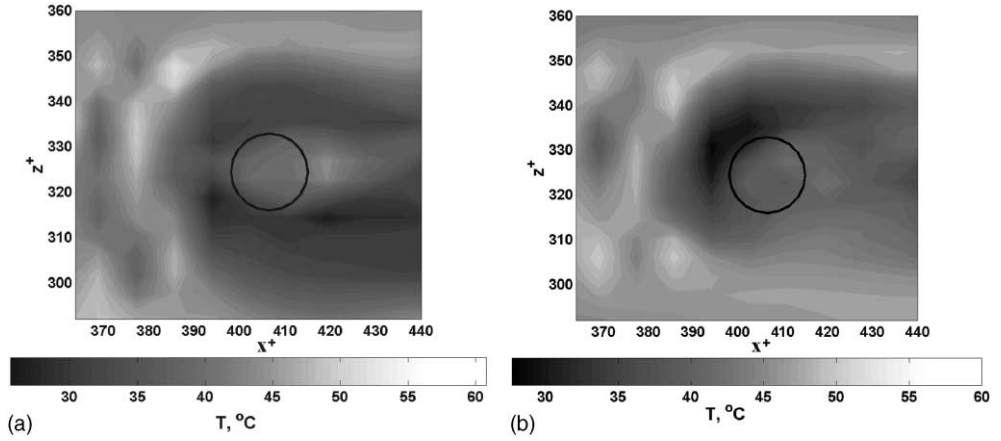


Fig. 3. Instantaneous temperature pattern on the heated wall in the vicinity of the sphere of $d^+ = 17$: (a) at time $t^+$, (b) at time $t^+ + \Delta t^+$.

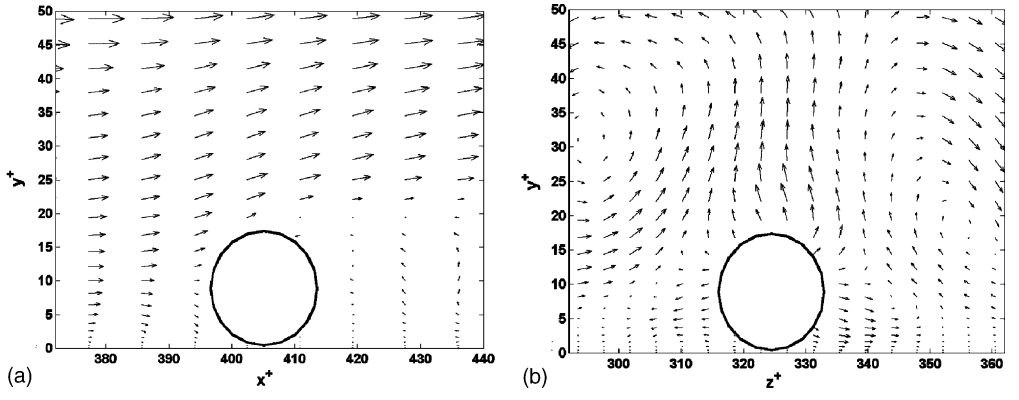


Fig. 4. Velocity around the sphere: (a) $x^+$–$y^+$ plane, (b) $z^+$–$y^+$ plane.

be defined: the flow along the sphere surface in the positive $y^+$ direction (measured from the front stagnation point) and flow in the negative $y^+$ direction. The flow in the positive $y^+$ direction accelerates from the front stagnation point and reaches a maximum velocity at the top of the sphere. The flow in the negative $y^+$ direction decelerates from the front stagnation point and reaches a zero velocity at the bottom. Recirculating flow behind the sphere is clearly seen. Velocity field (obtained simultaneously) in the $z^+$–$y^+$ plane is presented in Fig. 4b. The particle causes quasi-streamwise vortices, which detach a mass of fluid from the wall. When the sphere is on the bottom of the flume the deviations from its position are small. Calculations showed that the actual velocity field around the sphere deviated only slightly from that provided for sphere fixed to the bottom. The deposition determines the statistics of the temperature fields.

### 3.2. Statistics of temperature fields

#### 3.2.1. Profiles of the mean temperature

Fig. 5 shows the mean temperature profile for clear water and two types of particle-laden flow. Near the wall ($y^+ < 5$) the mean temperature profiles in particle-laden flow are equal to the clear water. However, for $y^+ > 5$ the results in Fig. 5 show differences in the particle-laden flow relative to the clean fluid. For $y^+ \geqslant 5$ the deviation of mean temperature profile for $d^+ = 17$ from profile of clear water is smaller compared to that for $d^+ = 8.5$. It should be taken into account that the ratio of the area occupied by particles, projected on the bottom wall, to the total bottom area (referred to as particle-occupation density) is smaller for particles of $d^+ = 17$. The effect of particle-occupation density was investigated experimentally by Kurose and Komori (2001). They showed that this parameter affects Reynolds stress and turbulence intensities outside the region occupied by particles. Our DNS showed that particle-occupation density affects also mean temperature profile.

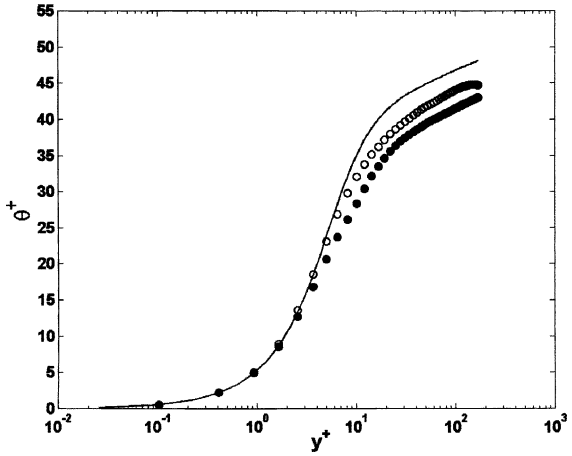


Fig. 5. Profiles of mean temperature: (—) clear flow, (●) $d^+ = 8.5$, (○) $d^+ = 17$.

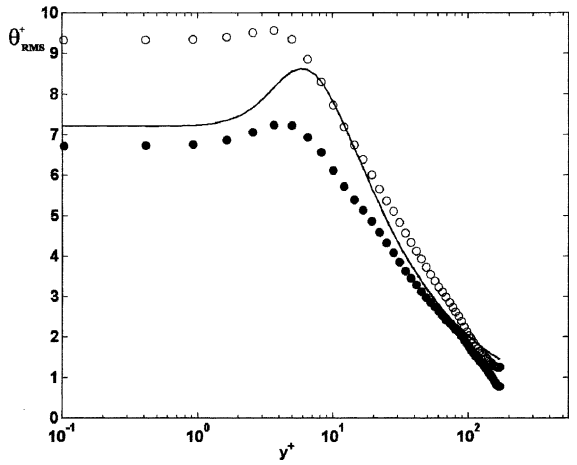


Fig. 6. RMS of temperature fluctuations: (—) clear flow, (●) $d^+ = 8.5$, (○) $d^+ = 17$.

### 3.2.2. Root-mean-square temperature fluctuations

The root-mean-square (RMS) of temperature fluctuations are shown in Fig. 6. The $\theta^+_{\mathrm{RMS}}$ does not change across the viscous sublayer. For moving particles ($d^+ = 8.5$) $\theta^+_{\mathrm{RMS}}$ is lower than that for clear water. For particles of $d^+ = 17$ the flow disturbances are stronger and $\theta^+_{\mathrm{RMS}}$ is higher compared to that for clear water.

### 3.2.3. Turbulent heat fluxes

Profiles of the axial and wall-normal heat fluxes are plotted in Fig. 7a and b. Addition of particles decreases axial turbulent heat flux compared to clear water. This effect is weaker for particles of $d^+ = 17$, when deposition occurs. Calculation results also show that peak values in particle-laden and clear flow occur at about the same values of $y^+$. Wall-normal turbulent heat flux increases with increasing values of $d^+$. This phenomenon results from the behavior of fluid

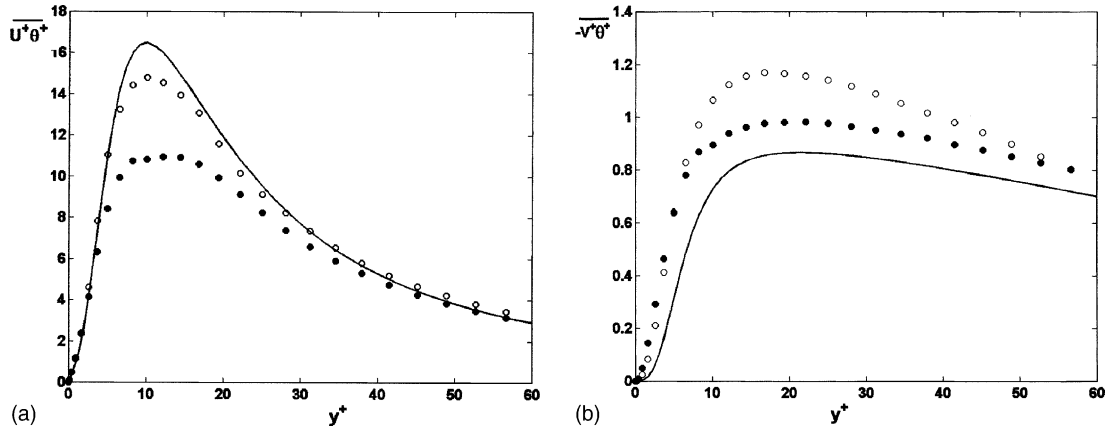


Fig. 7. Turbulent heat flux: (—) clear flow, (●) $d^+ = 8.5$, (○) $d^+ = 17$, (a) axial heat flux, (b) wall-normal heat flux.

velocity fluctuations. Li et al. (1999) reported that for particles $d^+ = 8.5$ and $d^+ = 17$ with density ratio $\rho = 1.05$ the wall-normal velocity fluctuations increase significantly compared to the clear flow. Unlike this case the stream turbulence intensities seem do not change significant in the near-wall region.

For heavy particles the effect of particles on turbulent intensities of carried fluid is opposite. Particle transport in fully-developed turbulent channel flow was investigated using LES by Wang and Squires (1996). For lycopodium, glass and copper particles it was demonstrated that the wall-normal velocity fluctuations were reduced while the streamwise values increased (see also Kulick et al., 1994).

### 3.2.4. Temperature–velocity correlation's

These are quantitative measures for interconnection between the thermal and kinematic characteristics of the turbulent fluctuations. Fig. 8 shows the behavior of correlation coefficient $R_{\theta u} = \overline{\theta^+ u^+}/\theta^+_{\mathrm{RMS}} u^+_{\mathrm{RMS}}$ of temperature and streamwise velocity fluctuations in the near-wall region for $d^+ = 8.5$ and $d^+ = 17$, respectively. The correlation coefficient in the flow with particles $d^+ = 8.5$ is higher than that in the flow with particles $d^+ = 17$. For the both size of the particles in the region $y^+ > 30$ the correlation coefficient almost does not change. The behavior of correlation coefficients $R_{\theta v} = \overline{\theta^+ v^+}/\theta^+_{\mathrm{RMS}} v^+_{\mathrm{RMS}}$ between fluctuations of wall-normal velocity and temperature shows that in particle-laden flow at $y^+ > 20$ $R_{\theta v}$ remains constant, Fig. 9.

### 3.2.5. Skewness factors of temperature fluctuations

The quantitative measure of the probability of departure of the temperature fluctuations from the Gaussian distribution is the skewness factor $S = (\theta^+)^3/(\theta^+_{\mathrm{RMS}})^3$. According to the basic assumption of the theory for small scale field isotropy (Corsin, 1951) all odd ordered moments should be zero. Fig. 10 shows the calculated $S$-factor for spherical particles of diameter $d^+ = 8.5$

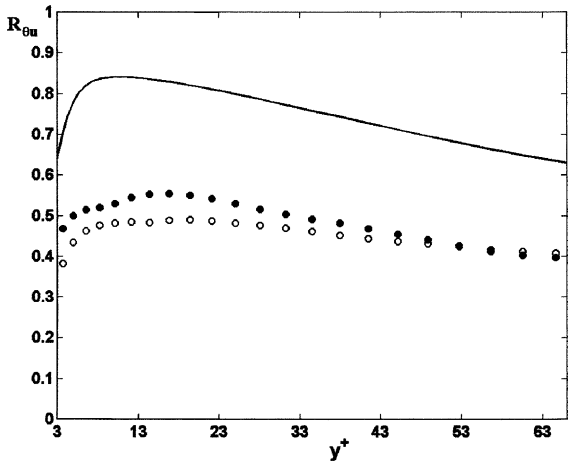


Fig. 8. Correlation coefficient between fluctuations of streamwise velocity and temperature: (—) clear flow, (●) $d^+ = 8.5$, (○) $d^+ = 17$.

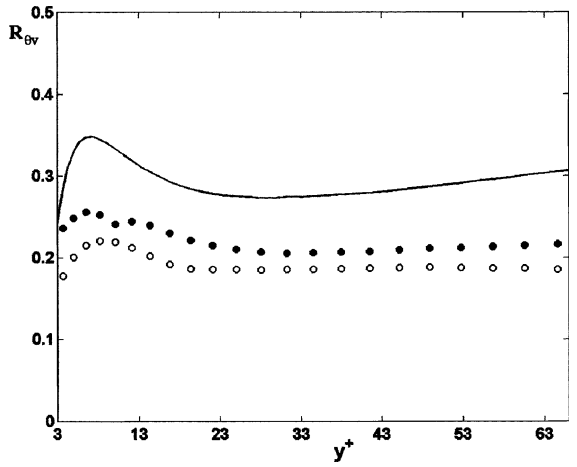


Fig. 9. Correlation coefficient between fluctuations of wall-normal velocity and temperature: (—) clear flow, (●) $d^+ = 8.5$, (○) $d^+ = 17$.

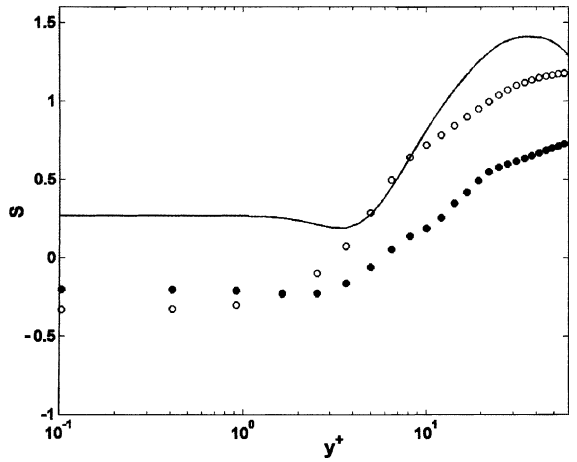


Fig. 10. Skewness factors of temperature fluctuations: (—) clear flow, (●) $d^+ = 8.5$, (○) $d^+ = 17$.

and $d^+ = 17$ versus dimensionless distance from the wall. The data presented in Fig. 10 indicate that the $S$-factors do not change in the region $y^+ < 1$ and are close to zero.

### 3.2.6. Two-point autocorrelations

Fig. 11 shows two-point autocorrelation functions of the streamwise velocity fluctuations in the streamwise direction calculated at the distance $y^+ = 4.9$ and $y^+ = 8.2$ for $d^+ = 8.5$ and $d^+ = 17$, respectively, from the bottom of the flume. The autocorrelation function decays close to zero for both clear water and particle-laden flow. The periodicity length, which is long enough for the velocity field of clear water flow is long enough also for the field of particle-laden flow. Fig. 12 shows the spanwise two-point correlation for streamwise velocity. For clear water the position of the minimum in the streamwise velocity correlation at ≈50 wall units shows the presence of the

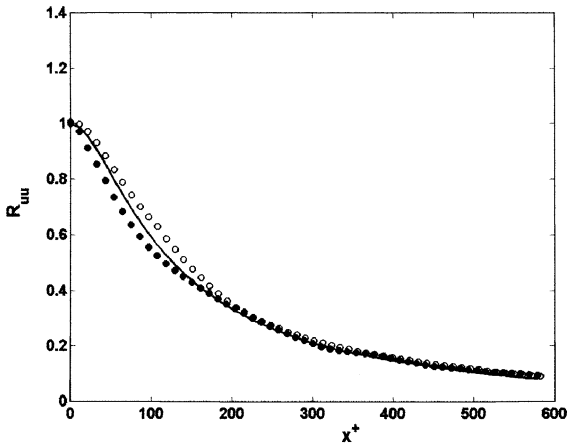


Fig. 11. Two-point autocorrelation $R_{uu}$ of streamwise velocity fluctuations at $y^+ = 4.9$ and $y^+ = 8.2$ for $d^+ = 8.5$ and $d^+ = 17$, respectively in the streamwise direction: (—) clear flow, (●) $d^+ = 8.5$, (○) $d^+ = 17$.

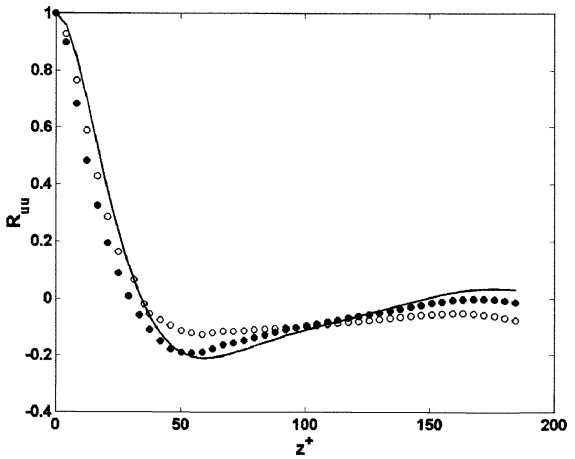


Fig. 12. Two-point autocorrelation $R_{uu}$ of streamwise velocity fluctuations at $y^+ = 4.9$ and $y^+ = 8.2$ for $d^+ = 8.5$ and $d^+ = 17$, respectively in the spanwise direction: (—) clear flow, (●) $d^+ = 8.5$, (○) $d^+ = 17$.

low-speed streaks with a typical spanwise distance of about 100 wall units. For particle-laden flow the position of the minimum is slightly shifted. In this case the low-speed streaks approximately, but not exactly, coincide with the clear water.

## 4. Experiments

In the DNS calculations discussed above, the resolution in the $x^+$–$z^+$ plane was $\Delta x^+ = 8.4$ and $\Delta z^+ = 4.2$. To clarify temperature distribution on the heated wall near the sphere with higher spatial resolution an experimental study was carried out.

### 4.1. Experimental facility

The bulk of experiments were performed in a flume described by Hetsroni et al. (1997), and only the main hydraulic parameters are presented here. The flow system is a stainless steel open flume 4.3 m long, 0.32 m wide and the flow depth was 0.037 m. The fluid mean temperature was maintained at 20 °C for all tests.

A fully developed flow was established in the region 2.5 m downstream from the inlet to the flume. The measurements of the water velocity profile and the distribution of the RMS values of streamwise velocity fluctuations confirmed this. Care was taken to eliminate vibration, wave formation at the inlet and reflections from the outlet.

The heated test section, Fig. 13, was located at the distance of 2.5 m from the channel entrance. The constantan heater (on an isolated frame) was made of a foil 0.33 m long, 0.2 m wide and 0.05 mm thick. Uniform heat flux was achieved by applying DC power to the heater. The surface temperature of the heater was affected by the turbulent flow over it and was measured by an IR imaging radiometer. The IR radiometer was situated under the heater so that outside wall temperature was measured. Hetsroni and Rosenblit (1994) have shown that the difference between the temperatures of the two sides of the wall i.e. the inside wall temperature and the outside wall temperature is less than 0.1 °C. The frequency response of temperature measurements was $f = 25\ \mathrm{s}^{-1}$.

### 4.2. Experimental procedure and accuracy of measurements

The sphere of density $1.050 \pm 0.005\ \mathrm{g/cm}^3$ was placed on the bottom of the test section. For conditions of present experiments dimensionless sphere diameter was $d^+ = 17$. Both IR and video images were obtained simultaneously. In a typical experiment, a series of two simultaneous images was acquired. Fig. 14a and b present the particle position (view from the top) and thermal pattern on the heated wall around the particle (view from below), respectively. The flow is from the right to the left. The dimensions in the streamwise and in the spanwise directions are 70 mm × 70 mm. These dimensions correspond to 256 pixels × 256 pixels. The number of frames counted for each series was 160. The images were processed to find the particle position and temperature distribution near the particle on the heated bottom wall. The spacial resolution was $\Delta x^+ = \Delta z^+ = 1.2$.

The experiments were performed under isoflux wall boundary condition, at heat flux $q = 3500$–$4000\ \mathrm{W/m}^2$. Electric power used for heating was measured with an accuracy of ±0.5%. The flow rate was measured with an accuracy of ±0.5%. The value of the Reynolds number $Re = u^*2H/\nu$ was $171 \pm 3$. The accuracy of the temperature measurements was ±0.1 °C.

The experimental values of time-averaged local heat transfer coefficients are defined as $\alpha = q(T_w - T_f)$ where $q$ is heat flux, $T_w$ is the time-averaged wall temperature at a given point, $T_f$ is the time-averaged mean value of bulk fluid temperature. The local values of $T_w$ at the given positions were determined from IR images shown in Fig. 14b using the TherMonitor image-processing software. The bulk fluid temperature was measured by thermometer.

The 95 confidence uncertainty calculated from the measurements heat transfer coefficient, $\delta\alpha/\alpha$, is given by the following combination of a random contribution to the uncertainty, $P$, and bias contribution, $B$, (the magnitude of the fixed, constant error). The random uncertainty calculated from the measurements was 0.03. The bias limits in the wall and fluid temperature measurements

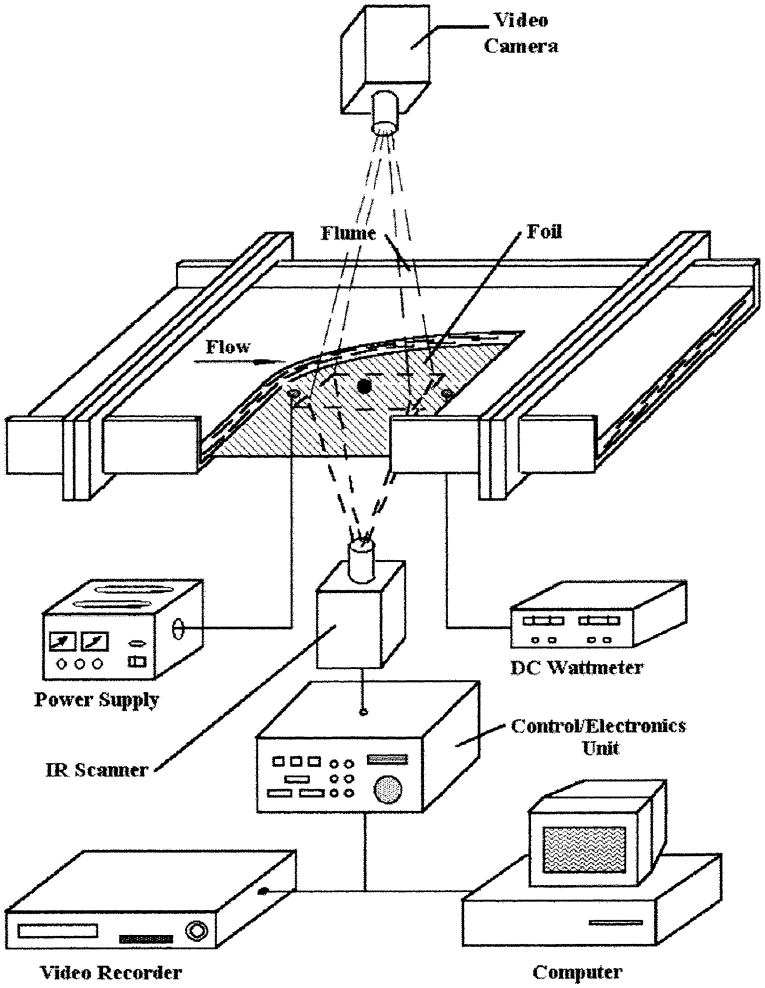


Fig. 13. Experimental setup.

are 0.1 K, the bias error of the mass flow meter system was 0.5%, the bias error of heat flux was 0.5%. For the mean value of temperature difference between heated wall and flow, $(T_w - T_f) = 15$ K the overall bias error is $B = 0.011$. Following the equation of Kline and McClintock (1953) the overall uncertainty in the determination of heat transfer coefficient is 0.033. IR technique provides high accuracy of determination of the local heat transfer coefficients. (For comparison, the local mass transfer coefficients reported by Braun et al. (1999) were determined with an accuracy of 0.041).

### *4.3. Heat transfer coefficients*

The normalized heat transfer coefficients along the axis of symmetry of the sphere in the streamwise direction are presented in Fig. 15. The normalization was performed with the time and space averaged heat transfer coefficient $\alpha_0$, which was derived from the average heat flux and

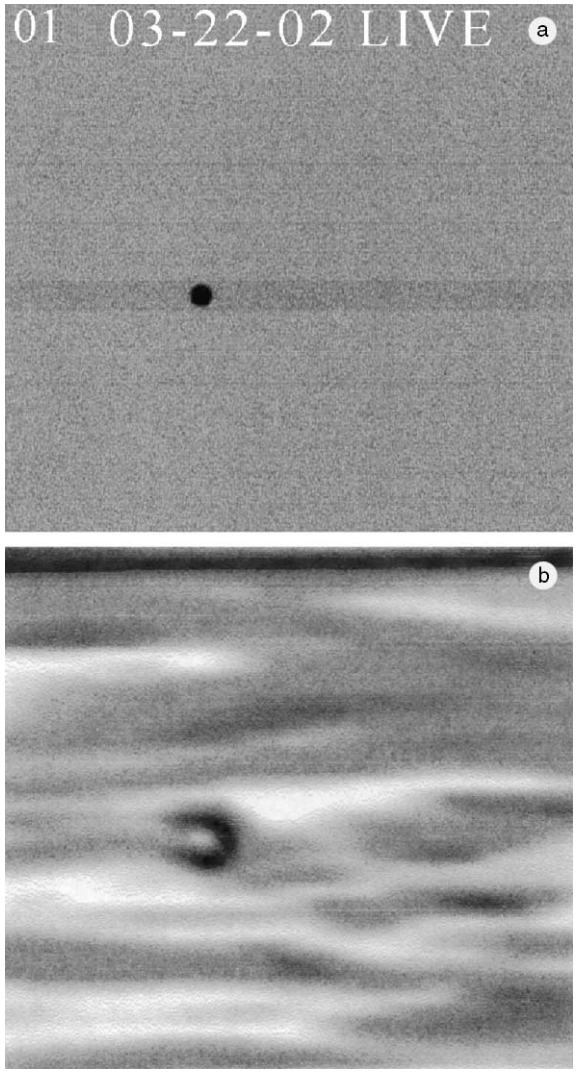


Fig. 14. Visualization of experiments: (a) particle position, (b) thermal pattern on the heated bottom of the flume.

bottom temperature without sphere. In the region located near the front of the sphere, $(x^+/d^+) \sim -0.5$, the rate of heat transfer is determined by strong flow toward the bottom (see Fig. 3a), which causes sharp growth of the heat transfer coefficient. Recirculating flow behind the sphere causes minimum of heat transfer coefficient at $(x^+/d^+) \sim -0.5$. Experimental results agree well with DNS calculations.

Normalized heat transfer coefficients $\alpha/\alpha_0$ across the width of the flume at different streamwise locations are presented in Fig. 16a–c vs. $z^+/d^+$ ($z^+$ is the spanwise distance from the initial position of the center of the sphere). The spanwise distribution of local heat transfer coefficients is close to symmetrical relatively to the point $(z^+/d^+) = 0$. For fixed sphere the symmetrical spanwise temperature distribution at the heated bottom were observed (Hetsroni et al., 2001b). One

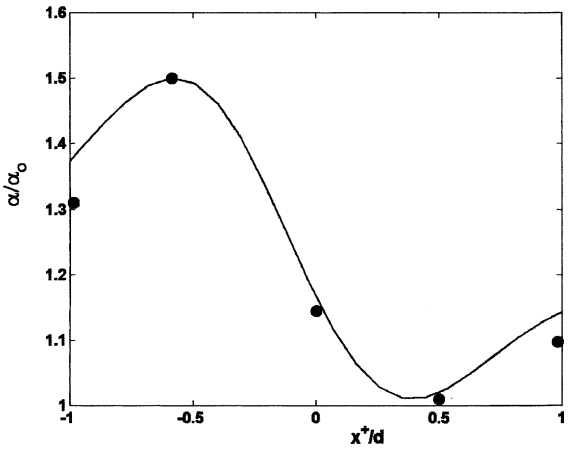


Fig. 15. Heat transfer coefficient near the sphere along streamwise symmetry line: (—) experiment, (●) DNS.

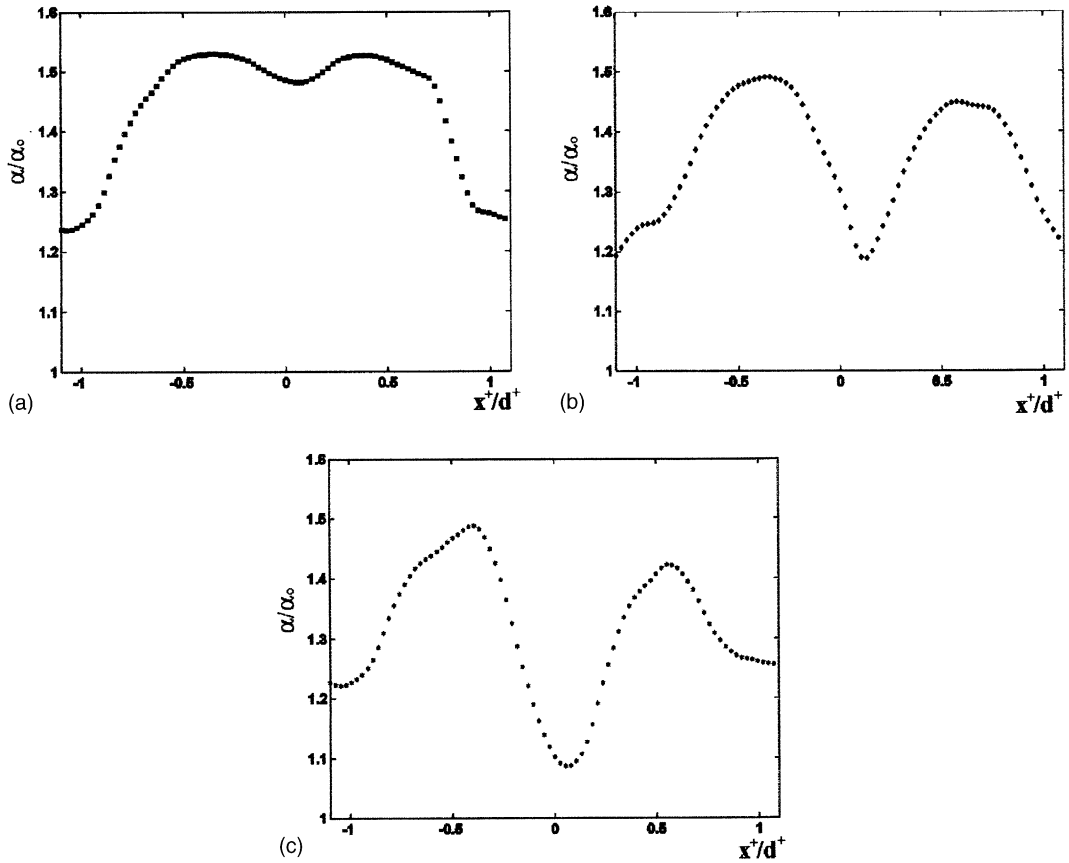


Fig. 16. Heat transfer coefficient near the sphere along spanwise cross-section lines: (a) $x^+/d^+ = -1/2$, (b) $x^+/d^+ = 0$, (c) $x^+/d^+ = 1/2$.

can conclude that the small displacement of the sphere contributes small, generally unimportant, changes in time averaged heat transfer coefficients compared to the sphere attached to the bottom.

## 5. Discussion

### 5.1. Particle deposition

We consider the lift force to clarify the effect of particle diameter on the behavior of a solid sphere on the bottom wall region of a flume. In previous studies, carried out for a small sphere in linear shear flows (Saffman, 1965; McLaughlin, 1991), the lift force has been considered to act from the lower-fluid-velocity side to the higher-fluid-velocity side and the value of the lift coefficient $C_L$ is positive. The negative value of $C_L$ means that the lift force acts from the higher-fluid-velocity side to lower-fluid-velocity side.

To estimate the lift force in a shear flow, Kurose and Komori (1999) derived the expression

$$C_L = 5.816\left(\frac{|\gamma^*|}{Re_p}\right)^{1/2} - 0.875\gamma^* \tag{16}$$

here $\gamma^*$ is the dimensionless shear rate of the fluid,

$$\gamma^* = \frac{d^+}{2U_C^+}\frac{\partial U^+}{\partial y^+} \tag{17}$$

and $U_C^+$ is the mean velocity of the fluid on the streamline through the center of the sphere normalized by the friction velocity $u^*$. In the present study for the sphere $d^+ = 17$, $Re_p = 120$, and the lift coefficient derived from Eq. (16) has a negative value (Hetsroni et al., 2001a,b). As is shown by Kurose and Komori (1999) the negative lift force is attributed to the flow separation behind the sphere, at high particle Reynolds numbers, $Re_p > 100$. The negative lift force together with the friction, result in particle deposition. The particle-turbulence interaction, in particular bursting process, causes particles oscillations around their initial locations.

From Eq. (17) one can conclude that $\gamma^*$ decreases with increasing $y^+$ and at the certain distance from the bottom of the flume $C_L$ becomes positive. The experimental observations also showed that when the sphere was placed far enough from the bottom, approximately at a distance $y^+ > 50$, it was moved by the flow. When the sphere was placed near the bottom, $y^+ < 30$, the sphere began to move but after certain time it stayed almost motionless.

### 5.2. Particle effects on scalar transfer

Campbell and Hanratty (1983) investigated the turbulent mass transfer at a solid wall and they concluded that the averaged mass transfer coefficient is related to the wall-normal velocity fluctuations. The experiments of Rashidi et al. (1990) and Kaftori et al. (1998) showed that the particle-turbulence interaction manifests itself in the change of a level of wall-normal turbulent fluctuations and bursting period. Particles may affect scalar transport in the near-wall region of a turbulent channel flow, particularly when the Prandtl number $Pr > 1$. With increasing Prandtl

number the resistance of heat transfer in the viscous sublayer increases. According to DNS carried out for clear flow by Tiselj et al. (2001) in the air flow about 25% of the total temperature difference between the temperature of the wall and that of the free surface occurs in the region $0 < y^{+5}$, whereas in the water flow with $Pr = 5.4$ it is two times higher (about 50%).

Hetsroni and Rosenblit (1994) reported the results of an experimental investigation on the solid particle effect on heat transfer in a turbulent flume. They found that the enhancement of heat transfer, due to the addition of particles, can reach as high as 35%, depending on particle size, particle loading and flow Reynolds number. The present DNS results show (Fig. 7b) that the addition of solid particles in turbulent boundary layer causes an increase in wall-normal turbulent heat flux. Subramanian et al. (1973) assumed that the enhancement of the heat transfer due to particles placed near the wall is caused by "film scraping" and "particle convection". The term "particle convection" means that while leaving the near-wall region, the particles themselves take the heat away to the bulk flow. "Particle convection" plays a dominant role in the heat transfer in gas-particle flows with a small size of particles. The significance of the "film scraping" begins to increase with the particle size or in particle-laden flow. For particles of $d^+ = 8.5$ used in the present study, this mechanism may also lead to enhancement of wall-normal turbulent heat flux.

We compare our experimental data for $d^+ = 17$ in flow of the bulk Reynolds number $Re_B = 2600$ with results for $d^+ = 9.6$ particles in flow of $Re_B = 5000$ presented by Hetsroni and Rosenblit (1994). We made this comparison because these two sets of data are the closest pair among all data reported by Hetsroni and Rosenblit (1994). Although this comparison is qualitative rather than quantitative, significant enhancement in heat transfer, in line with Hetsroni and Rosenblit's (1994) experiment is observed in our study.

## 6. Conclusion

The temperature distribution was investigated both by DNS and experimentally in particle-laden turbulent flow in a flume. Simulations were performed at $Re = 171$ and $Pr = 5.4$ in order to study the interaction between particle motion and flow turbulence. Two-way coupling was used to obtain various turbulence statistics, the grid resolution was sufficiently fine to resolve all essential turbulent scales. The coarse particles with density ratio close to unity were used in this study. Two different types of particle-turbulence interaction were considered: the first considers the effect of moving particles on surrounding flow and temperature field, the second considers this problem under condition of particle deposition. It should be taken into account the relation of the particle relaxation time to the time scale of fluid turbulence, $St^+$, and the relation of inertia to viscosity forces that act over the particles, $Re_p$. It follows that for the present study the particles located in the near-wall region rapidly deposit at $(Re_p/St^+) \sim 7$.

We have investigated the effect of nonuniform velocity field on turbulent heat transport. The study has been performed for two dimensionless diameters of spherical particles, $d^+ = 8.5$ and $d^+ = 17$. Surprisingly, for $d^+ = 17$ the effect of particles on profile of mean temperature and axial turbulent heat flux is weaker than that for particles of $d^+ = 8.5$. This is due to the fact that for particles of $d^+ = 17$ the deposition takes place.

The spatial structures of instantaneous flow and temperature fields were visualized. The low frequency small oscillations of deposited particles were observed. It was found that these small

deviations from the initial position may cause changes in the instantaneous temperature field near the particle and show that the coarse particles affect a essential fraction of the flow's mass and in turn modify the flow and temperature field.

The experiments provided detail investigation of temperature field on the heated wall in the region of particle radius. In the region near the front of the particle a sharp grows of heat transfer coefficient was observed. The experimental results agree well with computational predictions.

## Acknowledgements

This research was supported by a joint grant from the Center for Absorption in Science of the Ministry of Immigrant Absorption and the Committee for Planning and Budgeting of the Council for Higher Education under the framework of the Kamea Program.

E. Pogrebnyak was supported by the Center for Absorption in Science, Ministry of Immigrant Absorption.

## References

Armenio, A., Fiorotto, V., 2001. The importance of the forces acting on particles in turbulent flows. Phys. Fluids 13, 2437–2440.

Braun, H., Neumann, H., Mitra, N.K., 1999. Experimental and numerical investigation of turbulent heat transfer in a channel with periodically arranged rib roughness elements. Exp. Therm. Fluids Sci. 19, 67–76.

Campbell, J.A., Hanratty, T.J., 1983. Mechanism of turbulent mass transfer at a solid boundart. AIChE J. 29, 223–229.

Corsin, S., 1951. On the spectrum of isotropic temperature fluctuations in isotropic turbulence. J. Appl. Phys. 22, 469–481.

Eaton, J.K., Fessler, J.R., 1994. Preferential concentration of particles by turbulence. Int. J. Multiphase Flow 20, 169–209.

Fessler, J.R., Kulick, J.D., Eaton, J.K., 1994. Preferential concentration of heavy particles in a turbulent channel flow. Phys. Fluids 6, 3742–3749.

Gavrilakis, S., Tsai, H.M., Voke, P.R., Leslie, D.C., 1986. Direct and large eddy simulation of turbulence. In: Schumann, U., Friedrich, R. (Eds.), Notes on Numerical Fluid Mechanics, 15. Vieweg, Braunschweig, pp. 105–120.

Goldstein, D., Handler, R., Sirovich, L., 1993. Modeling a no-slip flow boundary with an external force field. J. Comput. Phys. 105, 354–366.

Gore, R.A., Crowe, C.T., 1991. Modulation of turbulence by a dispersed phase. Trans. ASME, J. Fluids Engng. 113, 304–307. Heat Fluid Flow 19, 482–491.

Hetsroni, G., Rosenblit, R., 1994. Heat transfer to a liquid–solid mixture in a flume. Int. J. Multiphase Flow 20, 671–689.

Hetsroni, G., Gurevich, M., Rozenblit, R., Yarin, L.P., Ziskind, G., 2001a. The effect of particle motion on the thermal structure and on the heat transfer. Int. J. Multiphase Flow 27, 393–413.

Hetsroni, G., Li, C.F., Mosyak, A., Tiselj, I., 2001b. Heat transfer and thermal pattern around a sphere in a turbulent boundary layer. Int. J. Multiphase Flow 27, 1127–1150.

Hetsroni, G., Rozenblit, R., Lu, D.M., 1995. Heat transfer enhancement by a particle on the bottom of the flume. Int. J. Multiphase Flow 21, 963–984.

Hetsroni, G., Rozenblit, R., Yarin, L.P., 1997. The effect of coarse particles on the heat transfer in a turbulent boundary layer. Int. J. Heat Mass Transfer 40, 2201–2217.

Kaftori, D., Hetsroni, G., Banerjee, S., 1998. The effect of particles on wall turbulence. Int. J. Multiphase Flow 24, 359–386.

Kasagi, N., Kuroda, A., Hirata, M., 1989. Numerical investigation of near-wall turbulent heat transfer taking into account the unsteady heat condition in the solid wall. J. Heat Transfer-Trans. ASME 111, 385–392.

Kasagi, N., Tomita, Y., Kuroda, A., 1992. Direct numerical simulation of the passive scalar field in a turbulent channel flow. Trans. ASME J. Heat Transfer 114, 598–606.

Kawamura, H., Ohsaka, K., Abe, H., Yamamoto, K., 1998. DNS of turbulent heat Transfer in channel flow with low to medium-high Prandtl number fluid. Int. J. Heat Fluid Flow 19, 482–493.

Kim, S., Karrila, S., 1991. Microhydrodynamics. Butterworth, London.

Kline, S.J., McClintock, F.A., 1953. Describing uncertainties in single-sample experiments. Mech. Engng. 75, 3–8.

Kulick, J.D., Fessler, J.R., Eaton, J.K., 1994. Particle response and turbulence modification in fully developed channel flow. J. Fluid Mech. 277, 109–134.

Kurose, R., Komori, S., 1999. Drag and lift force on a rotating sphere in a linear shear flow. J. Fluid Mech. 384, 183–206.

Kurose, R., Komori, S., 2001. Turbulence structure over a particle roughness. Int. J. Multiphase Flow 27, 673–683.

Lam, K.L., Banerjee, S., 1988. Investigation of turbulent flow bounded by a wall and a free surface. In: Michaelides, E.E., Sharma, M.P. (Eds.), Fundamentals of Gas–Liquid Flows, Vol. 72. ASME, Washington, pp. 29–38.

Li, C., Mosyak, A., Hetsroni, G., 1999. Direct numerical simulation of particle-turbulence interaction. Int. J. Multiphase Flow 25, 187–200.

Li, Y., McLaughin, J.B., Kontomaris, K., Portela, L., 2001. Numerical simulation of particle-laden turbulent channel flow. Phys Fluids 13, 2957–2967.

Lumley, J.L., Blossey, P., 1999. In: Salas, M.D., Hefner, J.N., Sakell, L. (Eds.), Modeling Complex Turbulent Flows. Kluwer Academic Publishers, Boston, pp. 89–106.

McLaughlin, J.B., 1989. Aerosol particle deposition in numerically simulated channel flow. Phys. Fluid A 1, 1211–1224.

McLaughlin, J.B., 1991. Inertial migration of a small sphere in linear shear flows. J. Fluid Mech. 224, 261–274.

Nino, Y., Garcia, M.H., 1996. Experiments of particle turbulence interactions in the near-wall region of an open channel flow: implications for sediment transport. J. Fluid Mech. 326, 285–319.

Pan, Y., Banerjee, S., 1996. Numerical simulation of particle interaction with wall turbulence. Phys. Fluids 8, 2733–2755.

Pan, Y., Banerjee, S., 1997. Numerical investigation of the effects of large particles on wall turbulence. Phys. Fluids 9, 3786–3807.

Pedinotti, S., Mariotti, G., Banerjee, S., 1992. Direct numerical simulation of particle behavior in the wall region of turbulent flows in horizontal channels. Int. J. Multiphase Flow 18, 927–941.

Rashidi, M., Hetsroni, G., Banerjee, S., 1990. Particle-turbulence interaction in a boundary layer. Int. J. Multiphase Flow 16, 935–949.

Saffman, P.G., 1965. The lift of a small sphere in a slow shear flow. J. Fluid Mech. 22, 385–400.

Subramanian, N.S., Rao, D.P., Gopich, T., 1973. Effect on heat transfer due to a particle in motion through thermal boundary layer over a flat plate. Inc. Eng. Chem. Fund. 12, 479–482.

Tiselj, I., Pogrebnyak, E., Li, C., Mosyak, A., Hetsroni, G., 2001. Effect of wall boundary condition on scalar transfer in a fully developed turbulent flume. Phys. Fluids 13, 1028–1039.

Wang, Q., Squires, K., 1996. Large eddy simulation of particle-laden turbulent channel flow. Phys. Fluids 8, 1207–1223.

White, F.M., 1991. Viscous Fluid Flow. McGraw-Hill, New York.

Yamamoto, Y., Potthoff, M., Tanaka, T., Kajishima, T., Tsuji, Y., 2001. Large-eddy simulation of turbulent gas-particle flow in a vertical channel: effect of considering inter-particle collisions. J. Fluid Mech. 442, 303–334.